Molecular Neurobiology (2022) 59:2563–2579
https://doi.org/10.1007/s12035-021-02679-1

Involvement of Paired Immunoglobulin-like Receptor B in Diabetes-Associated Cognitive Dysfunction Through Modulation of Axon Outgrowth and Dendritic Remodeling

Kairui Pu[1] · Meiyan Wu[1] · Tao Jiang[1] · Yuxin Zhang[1] · Mao Ye[1] · Jianyu Sun[1] · Hongli Ma[1] · Qian Zhai[1] · Qiang Wang[1]

Received: 1 September 2021 / Accepted: 1 December 2021 / Published online: 29 January 2022

Abstract

Type 2 diabetic patients have high risk of developing cognitive dysfunction, in which neural structural plasticity has played a pivotal role. Paired immunoglobulin-like receptor B (PirB), a receptor mainly expressed in neurons, acts as a critical inhibitor of neurite outgrowth and neural plasticity. However, the role of PirB in type 2 diabetes-associated cognitive dysfunction remains unknown. In this study, learning and memory impairment was observed in 24-week-old db/db mice by performing Morris water maze task, and the number of synapses along with the length of postsynaptic density by transmission electron microscopy were reduced in the hippocampus of db/db mice. Furthermore, PirB expression in the hippocampus of db/db mice was significantly upregulated using western blotting and immunofluorescence analysis. In cultured hippocampal neurons, high glucose treatment reduced the length of the longest neurite as well as axon initial segment (AIS), whereas silencing PirB expression rescued high glucose-induced neurite outgrowth inhibition, but not AIS. Additionally, cognitive deficits, dendrite morphology defects, and synapse-related proteins loss in db/db mice were alleviated when PirB knockdown was performed by adeno-associated virus injection. In conclusion, PirB is involved in diabetes-associated cognitive dysfunction through modulation of axon outgrowth and dendritic remodeling, providing a potential therapeutic target for diabetes-associated cognitive dysfunction.

Keywords Diabetes · Cognitive dysfunction · PirB · Neural structural plasticity · Hippocampus

Abbreviations

PirB	Paired immunoglobulin-like receptor B
AD	Alzheimer's disease
LTP	Long-term potentiation
LTD	Long-term depression
MWM	Morris water maze
AAV	Adeno-associated virus
RIPA	Radioimmunoprecipitation assay
SDS-PAGE	SDS-polyacrylamide gel electrophoresis
PVDF	Polyvinylidene fluoride
PSD	Postsynaptic density
AIS	Axon initial segment
PSD95	Postsynaptic density protein 95
MAP2	Microtubule-associated protein 2
βIII-tubulin	Class III beta-tubulin
Syp	Synaptophysin
α1-NaKA	α1 Subunit of Na+/K+-ATPase
GAP43	Growth-associated protein-43
RhoA	Ras homolog gene family member A
POSH	Plenty of SH3s

Introduction

Diabetes is a chronic metabolic disease affecting over 422 million people around the world. Converging evidence shows that type 2 diabetes has an increased risk of developing cognitive impairment (up to 60%) and dementia (50–100%) [1]. In particular, dementia has become the top 2 leading causes of diabetes-related death according to a recent epidemiological analysis [2]. It is clear that multiple risk factors, including hyperglycemia, insulin resistance, inflammation, and altered lipid mediators, are involved in diabetes-associated cognitive dysfunction, but the potential biological mechanisms are unknown [1, 3]. Given the very large increase in type 2 diabetes development worldwide

✉ Qiang Wang
dr.wangqiang@139.com

[1] Department of Anesthesiology & Center for Brain Science, The First Affiliated Hospital of Xi'an Jiaotong University, Xi'an 710061, Shaanxi, China

[4], combined with aging populations, identifying the precise mechanisms underlying diabetes-associated cognitive dysfunction is of great importance.

Impaired neural plasticity is implicated in cognitive dysfunction of neurodegenerative diseases [5, 6]. Studies on diabetes have reported spine density reduction and synapse-related proteins loss, including postsynaptic density protein 95 (PSD95) and microtubule-associated protein 2 (MAP2), in the hippocampus and prefrontal cortex of db/db mice [7–9]. Furthermore, synaptic efficiency has been shown to be impaired in the dentate gyrus and CA1 region of diabetic mice, accompanied by lower basal levels of Ca^{2+}/calmodulin-dependent protein kinase II activity [10–12]. Given that structural plasticity is directly associated with synaptic and cognitive function, therapeutic strategies aiming to preserve the integrity of neural structural plasticity may be beneficial in treating diabetes-associated cognitive dysfunction.

Paired immunoglobulin-like receptor B (PirB), a cell-surface receptor mainly expressed in neurons, is implicated in neurite outgrowth and restricting neural plasticity [13, 14]. Most studies focused on the visual cortex have reported that loss of PirB leads to higher functional synapse frequency and spine density of pyramidal neurons even beyond the critical period of brain development [15–17]. Similar results were also found in another brain region, i.e., -hippocampus, including deficient long-term depression (LTD) and increased long-term potentiation (LTP) accompanied by better performance of learning and memory tasks in loss-of-PirB-function mice [18, 19]. Moreover, PirB was found as a high-affinity receptor for Aβ oligomers and their bindings promoted synaptic loss and cognitive deficits in Alzheimer's disease (AD) [19]. These findings prompt investigations into the role of PirB deficiency in neuroprotective effects of diabetes.

Our previous study demonstrated that cerebral ischemic-reperfusion induces PirB expression elevation in the cortical penumbra, which inhibited axon outgrowth by targeting downstream signaling molecules of growth-associated protein-43 (GAP43), plenty of SH3s (POSH), and ras homolog gene family member A (RhoA) [20, 21]. Furthermore, PirB upregulation was also observed in aging mice, further supporting the role of PirB in aging-related cognitive decline. In this study, we investigated that whether PirB receptor expression is upregulated in diabetic brains and whether it is involved in the modulation of neural structural plasticity and cognitive dysfunction in diabetes.

In this study, we used db/db mice as the animal model to assess cognitive function by Morris water maze (MWM). To investigate the role of PirB in diabetes-induced synaptic and cognitive impairments, we detected PirB expression in the hippocampus and cultured primary neurons exposed to high glucose or osmotic control. Furthermore, we used recombinant lentiviral vectors or adeno-associated virus (AAV) to knock down PirB expression in vitro and in vivo respectively. Immunofluorescence and Golgi staining were used to observe neurite outgrowth and dendritic morphology in the presence or absence of PirB. This study highlights PirB as a key player in negative effects on hippocampal neuroplasticity from diabetes and provides a potential target for treatment.

Materials and Methods

Animals

All animal experiments were approved by the Institutional Animal Care and Use Committees of Xi'an Jiaotong University (Xi'an, China; 2019–060) in accordance with the National Institutes of Health guidelines. Homozygous leptin receptor-deficiency male mice (db/db) on C57BLKS background and littermate control (m/m) were purchased from the Model Animal Research Center of the Nanjing University (Nanjing, China). All animals were kept in groups of 2–4 individuals with ad libitum access to water and food pellets in a 12-h light/dark cycle. Blood glucose and body weight were recorded once a week. AAV injections were performed into the bilateral hippocampus of 16 weeks animals. After 8-week recovery period, a battery of behavior tests and pathological analyses were carried out. Db/db mice with random blood glucose levels < 200 mg/dl were excluded during the experiments. Behavior tests were performed between 2:00 pm and 6:00 pm, and all the animals were handled twice a week before the beginning of the experiments.

Morris Water Maze

MWM paradigm was carried out to assess hippocampal-dependent spatial memory. The apparatus consists of a large round pool divided into 4 quadrants by phantom lines and a 10-cm-diameter platform hidden 1 cm beneath the surface of the water. The temperature of water was maintained at 22℃. The walls around the pool were pasted with the surrounding extra-maze visual cues to provide spatial cues for the animal. The behavior tests were divided into acquisition trials and probe test. During the acquisition phase, mice have received 4 training trials per day for 5 consecutive days, for 90 s each trial with at least 30-min interval. The escape latency was defined as the time that the mice spent reaching the hidden platform. During the probe phase, the last day of testing, the platform was removed. The mice were released in the second quadrant and the time spent in the target quadrant was recorded in limited 60 s. Path efficiency was calculated as follows: path efficiency = straight-line distance from start to platform/the path taken by the mouse. All

trials were monitored with the Tracking software (Taimeng, Chengdu, China).

Stereotactic Injection of Adeno-Associated Virus

rAAV-U6-shRNA(PirB)-CMV-mCherry-pA (virus titer: $\geq 2.0010^{12}$ vg/mL) and rAAV-U6-shRNA(scramble)-CMV-mCherry-pA (virus titer: $\geq 2.0010^{12}$ vg/mL) were purchased from BrainVTA (Wuhan,China). Briefly, all surgical procedures were performed under general anesthesia using isoflurane (2–3% vaporized in oxygen). The mice were placed in a stereotaxic frame (RWD) and performed a small craniotomy using a 1 mm gauge drill bit at the following coordinates: anteroposterior + 2.3 mm, mediolateral ± 2.3 mm, and dorsoventral − 2.05 mm. Then, 0.8 µL (per hippocampus) of either AAV-PirBi or AAV-vector was injected using a 10 µL Hamilton microsyringe at a rate of 0.04 µL/min and the needle was left in place for an additional 5 min before being retracted. Betadine and topical lidocaine were applied to the top of the suture to prevent infection and for analgesia. Animals were allowed to recover on a heating pad before returning to their home cages. Behavioral experiments were conducted after 8 weeks and then animals were sacrificed by decapitation under isoflurane anesthesia.

Primary Hippocampal Neuronal Cultures

The E16 embryonic hippocampus was isolated from sacrificed pregnant C57BL/6 mice, and then meninges were removed in ice-cold HBSS. Tissues were dissociated in 0.25% trypsin, triturated, centrifuged, and resuspended in medium (Neurobasal, B27 supplement, 2 mM L-glutamine, N-2 supplement, penicillin/streptomycin). Then the cells were counted using a hemocytometer and plated on poly-D-lysine-coated glass coverslips (10,000 cells/12 mm) or 6-well plates (100,000 cells/well). Cells were maintained at 37℃ with 5%CO2 in a humidified incubator. Fifty percent of media change was performed every third day. After 7 days in culture, high glucose culture medium (900 mg/dl) was used to stimulate primary hippocampal neurons for 3 days. Mannitol was used as an osmotic control.

Lentiviral Knockdown Experiments

To knock down PirB expression, we constructed two lentiviral shRNA vectors containing different shRNA sequences against PirB(sh1:5-AACAUCGAUAUUGACCUGCAUU-3; sh2:5-AACAAUAACAGCGAUAUUGCCC-3), as previous study [22]. The primary neurons were seeded at a density of 80% and were transfected with PirB siRNA (PirB-RNAi) or scrambled control siRNA (scramRNAi) at DIV4 followed by maintained for 24 h. Immunofluorescence and western blot analysis confirmed robust infection efficiency 3 days after the transfection.

Western Blot

Total proteins from cells and hippocampus were extracted in radioimmunoprecipitation assay (RIPA) lysis buffer (Beyotime). After determination of protein concentration with bicinchoninic acid method (ThermoFisher), 50 µg of total proteins were separated by SDS–polyacrylamide gel electrophoresis (SDS-PAGE) and transferred to polyvinylidene fluoride (PVDF) membranes. Then, the membranes were incubated with 5% skimmed milk buffer to prevent nonspecific binding of the antibodies. After that, primary antibodies: PirB (R&D Systems, Cat#AF2754), Synaptophysin1 (Synaptic Systems, Cat#101,011), PSD95 (Cell Signaling Technology, Cat#3450), GAP43 (Abcam, Cat#ab75810), and POSH (Santa Cruz Biotechnology, Cat#sc-100815) were used. The immunoreactive bands were visualized with an enhanced chemiluminescence reagent, and the intensity of bands was analyzed by Image J software.

Immunofluorescence Staining

Animals were anesthetized and perfused with 4% paraformaldehyde; brains were post-fixed 6 h and then dehydrated in 30% sucrose for 2 days. Frozen Sects. (16 µm thick) were cut coronally through the forebrain and mounted onto gelatin-coated slides. Primary hippocampal neurons were fixed in 4% paraformaldehyde for 10 min at room temperature. The brain sections or cell climbing slices were washed with PBS and blocked with 3%BSA diluted in PBS/0.2% Triton X-100 for 30 min at 37℃. Primary antibodies, NeuN (Millipore, Cat#MAB377), PirB (Invitrogen, Cat#MA5-29,749), PSD95 (Cell Signaling Technology, Cat#3450), βIII-tubulin (Abcam, Cat#ab78078), Synaptophysin1 (Synaptic Systems, Cat#101,011), AnkyinG (Santa Cruz Biotechnology, Cat#sc-12719), and MAP2 (Cell Signaling Technology, Cat#4542) were used overnight at 4℃. On the next day, the sections or cell climbing slices were incubated with Alexa Fluor 647, 488, or 594 donkey anti-mouse/rabbit/goat secondary antibodies (Invitrogen) for 2 h. Sections were imaged under a confocal microscope (Leica TCS SP8 STED 3X or Nikon A1 +) and analyzed by the Image J software.

Transmission Electron Microscopy

The hippocampus was carefully separated and rapidly cut into small pieces (1 mm^3) and then was fixed in 2.5% glutaraldehyde in PBS and post-fixed in 1% OsO4 at 4 °C. After fixation, samples were dehydrated in a graded series of alcohol and embedded upon Poly/Bed 812 resin followed by ultrathin (80-nm) sections with an ultramicrotome. Images

were generated with a Hitachi H-7650 transmission electron microscope (Hitachi, Japan) at 80 kV. Fifteen visual fields of each tissue section were imaged (15,000×) as a low-resolution map for quantitative analysis and then high-resolution images (400,000×) were captured to yield high-resolution images. The number of synapses and the length of postsynaptic density (PSD) were measured using Image J software. All electron microscopy quantification was performed blind to genotype by at least two independent observers.

Golgi Staining and Image Analysis

Twenty-four weeks of diabetic and control mice treated with AAV injection were sacrificed, and Golgi staining was conducted using the FD Rapid Golgi Stain Kit (FD NeuroTechonologies). Freshly dissected brains were quickly rinsed in PBS, transferred to impregnation solution, and kept in the dark at room temperature. After around 2 weeks, the brains were then transferred into solution C and stored in the dark at 4℃ for 72 h. Two hundred micrometer brain sections were cut with a vibratome and stained with Solution D and Solution E. Images from hippocampal regions were collected using a confocal microscope (Nikon A1 +). Dendrites were traced from the soma to the projection terminus using the Neuron J plug-in on Fiji (Image J). The Sholl analysis defines dendritic complexity by the number of dendritic branch points at fixed intervals from the cell bodies and was conducted using the Sholl analysis plug-in. Tertiary or greater order apical and basal dendrites were selected and spine densities were calculated from individual segment of dendrite greater than 10 μm in length.

Statistical Analysis

Statistical analyses were performed with GraphPad Prism 7 software. All values, except for sholl interaction (means + 95% confidence interval), are presented as mean ± SD. No formal a priori statistical power calculations were conducted, and the sample sizes were based on our previous knowledge and experience with this design. Data analyses were blinded to the experimenter. For western blot, PSD length, synapse frequency, AIS length, length of the longest neurite, total dendritic length, spine density, and quadrant time (%) were assessed by unpaired two-tailed student *t*-tests or one-way ANOVA followed by the Tukey post hoc test. Behavior tests and sholl interaction were assessed by two-way ANOVA followed by Bonferroni's or Tukey's post hoc analysis. $P < 0.05$ was considered as significance.

Results

24-Week-Old db/db Mice Developed Cognitive Deficits and Synaptic Injury

Hippocampal-dependent spatial memory was assessed using the MWM paradigm (Fig. 1b). During the acquisition phase, 24-week-old db/db mice displayed a slower learning performance on finding the hidden platform than m/m mice, which was demonstrated by significantly increased escape latency ($F_{(1,120)} = 47.08$, two-way ANOVA; post hoc analysis: days 2, $P = 0.0025$; days 3, $P = 0.0130$; days 4, $P = 0.0007$; days 5, $P = 0.0008$; Fig. 1c). However, swimming speed of db/db mice was significantly lower than m/m group during the test ($F_{(1,120)} = 45.94$, two-way ANOVA; post hoc analysis: days 1, $P = 0.0237$; days 2, $P = 0.0066$; days 3, $P = 0.0119$; days 4, $P = 0.0081$; days 5, $P = 0.0433$; Fig. 1d). To avoid interference from swimming speed difference between the two groups, we carried out path efficiency, a measure that is not sensitive to changes in swimming speed. Path efficiency of db/db mice was also lower compared to their m/m mice counterpart ($F_{(1,119)} = 20.5$, two-way ANOVA; post hoc analysis: days 2, $P = 0.0127$; days 5, $P = 0.0161$; Fig. 1e). Also, during the probe test, db/db mice displayed impaired retention ability compared to m/m group, as indicated by a lower percentage of time spent in the target quadrant (m/m: 28.49 ± 6.471% vs db/db: 18.38 ± 5.34%, $t_{(24)} = 4.341$, two-tailed unpaired *t*-test, $P = 0.0002$; Fig. 1f). These results suggested a serious impairment of cognitive function in 24-week-old db/db mice.

Next, we assessed the synaptic integrity of hippocampal neurons by electron microscopy analysis. Compared with m/m group, the number of synapses was significantly reduced in pyramidal neurons of db/db mice relative to m/m group (m/m: 75.11 ± 26.57/100 μm^2 vs db/db: 45.67 ± 10.26/100 μm^2, $t_{(16)} = 3.102$, two-tailed unpaired *t*-test, $P = 0.0069$; Fig. 1j) and the length of PSD was also shorter than m/m group (m/m: 0.3313 ± 0.03055 μm vs db/db: 0.2597 ± 0.02388 μm, $t_{(16)} = 5.54$, two-tailed unpaired *t*-test, $P < 0.0001$; Fig. 1h-1,2 and i). In higher magnification images of diabetic brain slices, we observed that the postsynaptic membranes were swollen, and synaptic clefts were blurred or missing at synaptic sites (Fig. 1h-4). However, in m/m group, the presynaptic and postsynaptic membranes were clear and had complete outlines, the synaptic cleft was clear, and abundant PSD was detected (Fig. 1h-3). These findings showed that synaptic morphology in the hippocampus was damaged in 24-week-old db/db mice, which is in line with the above observed behavioral abnormalities.

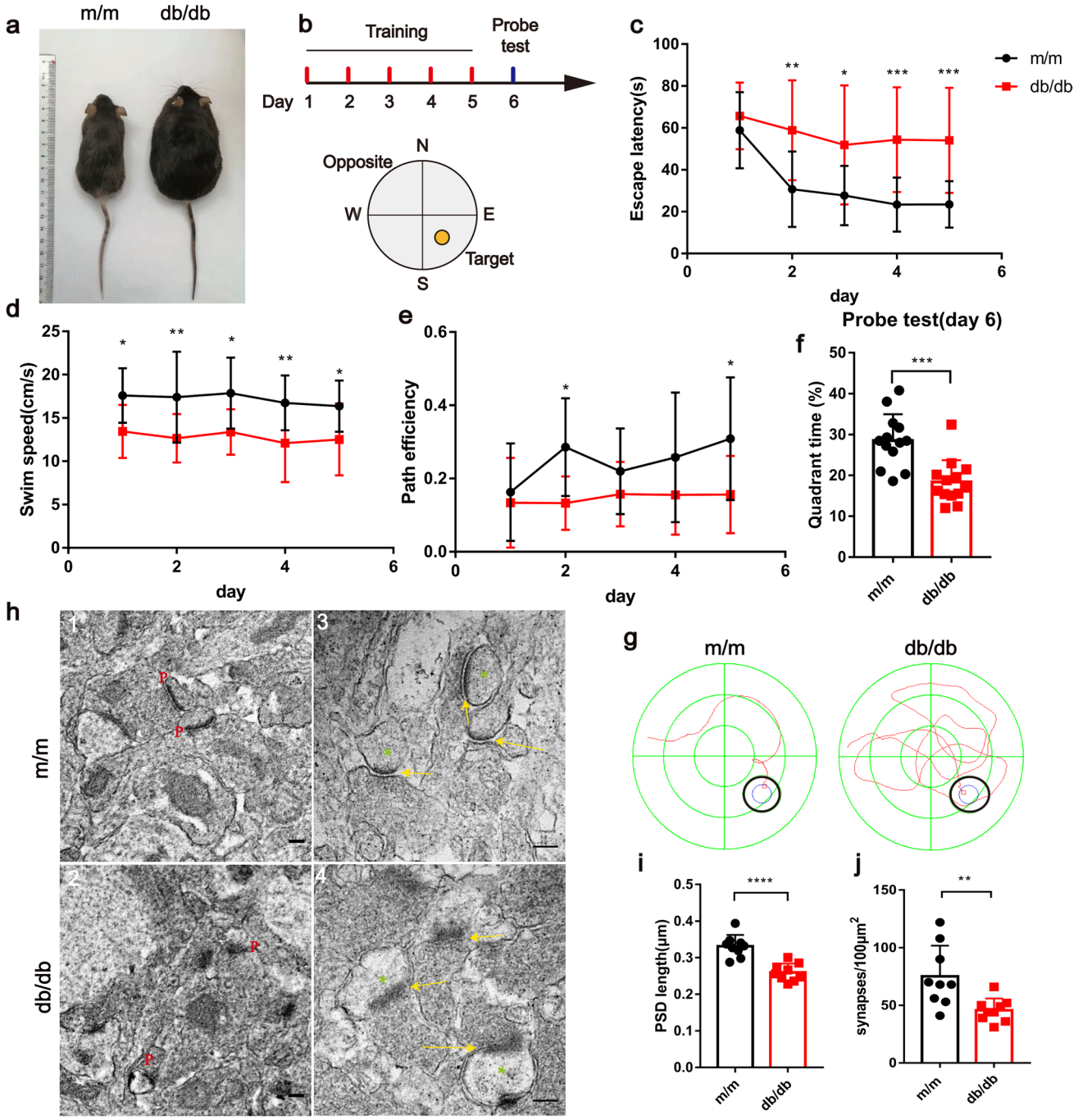

Fig. 1 Cognitive deficits and synaptic injury in 24-week-old db/db mice. **a** Overview of experimental mice. **b**–**g** Results of MWM test in 24-week-old db/db mice and their littermate control. Schematic diagram of MWM protocol (**b**). Escape latency (**c**), swim speed (**d**), and path efficiency (**e**) in the training session of MWM test. $n = 13$/group. $^{*}P < 0.05$, $^{**}P < 0.01$, $^{***}P < 0.001$ determined by two-way ANOVA with Bonferroni's multiple comparisons tests. **f** Time in the target quadrant during the probe trial on the last day of MWM test. $n = 13$/group. $^{***}P < 0.001$ determined by Student *t*-test. **g** Representative traces of db/db or m/m mice from MWM test. **h** Representative images of synaptic ultrastructure, including PSD (p), synaptic clefts (yellow arrow), and postsynaptic membrane (green asterisks) in the hippocampus. Scale bar, 0.2 μm. **i**–**j** Quantification of the length of PSD and synapse frequency. $n = 9$ from three mice per group. $^{**}P < 0.01$, $^{****}P < 0.0001$ determined by Student *t*-test. Data represent means ± SD. PSD, postsynaptic density

PirB Expression Was Upregulated in the Hippocampus of db/db Mice and High Glucose-Treated Primary Hippocampal Neurons

To determine whether PirB are related to the diabetes-associated cognitive dysfunction, we detected PirB protein expression upon high glucose exposure. Primary hippocampal neurons treated with high glucose (900 mg/dl) for 72 h exhibited increased apoptosis and decreased cell viability (data were not shown), whereas neurons treated with osmotic mannitol as control showed no apparent changes, supporting high glucose induces cytotoxic in primary neurons. Western blotting revealed that PirB protein level was increased upon high glucose exposure relative to the control group (fold change: 6.695 ± 3.075, t(4) = 4.233, two-tailed unpaired t-test, P = 0.0133; Fig. 2a–b).

This finding was further verified in db/db mice. Consistently, protein expression of PirB was elevated within the hippocampus of db/db mice (fold change: 1.769 ± 0.4087, $t_{(4)} = 4.641$, two-tailed unpaired t-test, $P = 0.0097$; Fig. 2c–d). This observation was further confirmed by immunofluorescence labeling of PirB and NeuN in hippocampal slices ($t_{(17)} = 3.224$, two-tailed unpaired t-test, $P = 0.0050$; Fig. 2e–f). POSH is an SH3-containing scaffold protein, acting as an intracellular signal transducer of PirB. We also detected that POSH protein was elevated (fold change: 2.807 ± 1.207, $t_{(4)} = 3.719$, two-tailed unpaired t-test, $P = 0.0205$) and axon growth marker GAP43 expression was decreased (fold change: 1.264 ± 0.09244, $t_{(4)} = 5.61$, two-tailed unpaired t-test, $P = 0.0050$) in the hippocampus of db/db mice compared to m/m group (Fig. 2g–j). However, we did not observe RhoA protein level changes ($t_{(4)} = 1$, two-tailed unpaired t-test, $P = 0.3739$; Fig. 2k–l). These results suggest that PirB signal pathway, but may not refer to RhoA, might be involved in cognitive dysfunction of diabetic mice.

Neurite Outgrowth Was Inhibited in High Glucose-Treated Primary Hippocampal Neurons

To determine whether the neurite outgrowth of primary hippocampal neurons is inhibited under high glucose condition, we performed immunostaining for class III beta-tubulin (βIII-tubulin), an axonal marker, and observed that the longest neurite length in the high glucose group was shorter than that in the control group (control: 306.5 ± 141.4 μm vs HG: 216.2 ± 91.92 μm, $t_{(75)} = 3.133$, two-tailed unpaired *t*-test, $P = 0.0025$; Fig. 3a–b).

Since previous studies have reported that the length of axon initial segment (AIS), a key structure for neuronal output that sits at the base of axon, is reduced in both hippocampus and prefrontal cortex of db/db mice [23, 24]. To gain insights into whether this structural region of axon is affected upon high glucose stimulation, we measured the AIS length by immunostaining of the AIS structural protein ankyrinG and found ankyrinG-positive segment was significantly shortened in the high glucose group (control: 27.58 ± 12.27 μm vs HG: 19.89 ± 8.347 μm, $t_{(134)} = 4.257$, two-tailed unpaired *t*-test, $P < 0.0001$; Fig. 3c–d). Taken together, these results suggested that neurite outgrowth was inhibited, and AIS length was significantly shortened under high glucose condition.

PirB Depletion Alleviated the Inhibitory Effect of Neurite Outgrowth in High Glucose-Treated Primary Hippocampal Neurons

To investigate the role of PirB in the regulation of neurite outgrowth, we transfected primary hippocampal neurons with recombinant lentiviral vectors containing PirB shRNA (PirB-RNAi) or non-silencing sequence (scramRNAi). Transfection efficiency was greater than 80%, determined by western blotting and immunofluorescence assay (Fig. 4a). In the HG + PirB-RNAi group, the longest neurite length was greatly enhanced by the suppression of PirB (HG + scramRNAi: 191.6 ± 71.06 μm vs HG + PirB-RNAi: 283.8 ± 102.5 μm, $t_{(69)} = 4.344$, two-tailed unpaired *t*-test, $P < 0.0001$; Fig. 4c–d). And following PSD95 immunofluorescence assay, we found that PirB-deficient neurons displayed less loss of synaptic PSD95-positive puncta that colocalize with neurite than scramRNAi-treated cells (Fig. 4b). To further determine whether PirB contributes to AIS shortening, we assessed AIS length after PirB depletion in high glucose-treated primary neurons. However, there was no difference between the two groups, indicating that AIS shortening might not attribute to the elevation of PirB (HG + scramRNAi: 36.62 ± 12.74 μm vs HG + PirB-RNAi: 39.19 ± 14.07 μm, $t_{(146)} = 1.165$, two-tailed unpaired *t*-test, $P = 0.2459$; Fig. 4e–f). Above all, these results indicated that PirB contributed to the inhibition of neurite outgrowth and synapse-related proteins loss in high glucose condition, but might not participate in AIS shortening.

PirB Depletion Rescued Synapse-Related Proteins Loss and Dendritic Morphology Defects in the Hippocampus of db/db Mice

To assess the effect of PirB deficiency on diabetes-induced synaptic dysfunction, we stereotactically injected AAV-PirBi or AAV-vector into both sides of hippocampus of 16-week-old db/db mice as well as age-matched littermates (Fig. 5a). Eight weeks later, mice were sacrificed after behavioral tests and brains were prepared for immunohistochemistry and proteins analysis. During this period, body weight and blood glucose were not significantly altered in db/db or m/m mice (Table1).

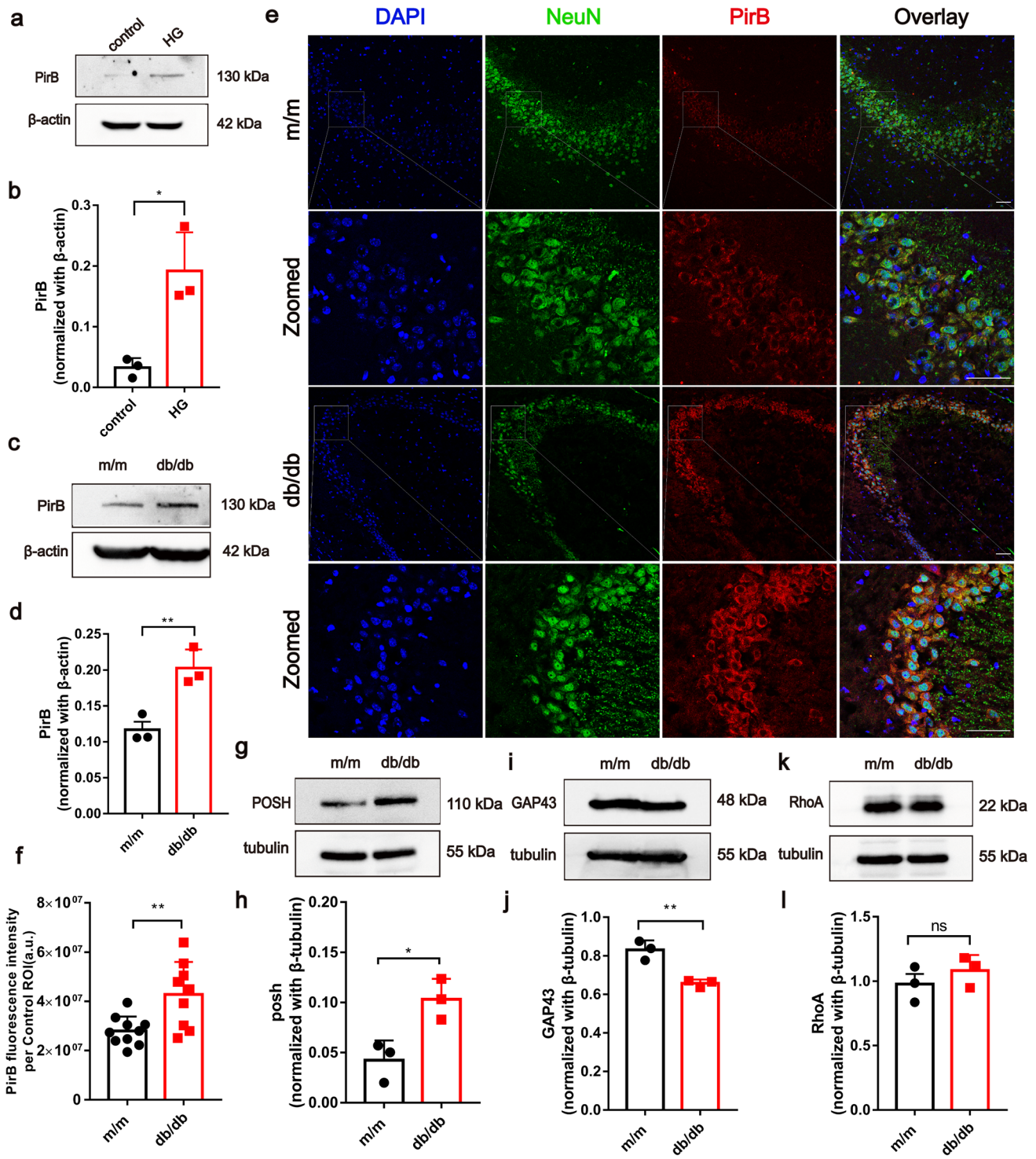

Fig. 2 PirB expression in the primary neurons exposed to high glucose and the hippocampus of db/db mice. **a**–**b** Western blots (**a**) with quantitative results (**b**) of PirB in primary hippocampal neurons treated with 900 mg/dl glucose or isotonic mannitol for 72 h. Data were collected from three independent experiments. $^{*}P<0.05$ determined by Student *t*-test. **c**–**d** Western blots (**c**) with quantitative results (**d**) show PirB protein expression in the hippocampus of 24-week-old db/db or m/m mice. $n=3$. $^{**}P<0.01$ determined by Student *t*-test. **e**–**f** Representative immunofluorescence images (**e**) with quantitative results (**f**) for PirB (red) and NeuN (green) in the hippocampus. m/m: $n=10$, db/db: $n=9$ from three mice per group. $^{**}P<0.01$ determined by Student *t*-test. Scale bar, 50 μm. **g**–**l** Western blots (**g**, **i**, **k**) with quantitative results (**h**, **j**, **l**) show downstream signaling molecules of POSH, GAP43, and RhoA in the hippocampus. $n=3$. $^{*}P<0.05$, $^{**}P<0.01$ determined by Student *t*-test. Data represent means ± SD. PirB, Paired immunoglobulin-like receptor B; POSH, Plenty of SH3s; GAP43, Growth associated protein-43; RhoA, Ras homolog gene family member A; NeuN, Neuronal nuclei; HG, high glucose

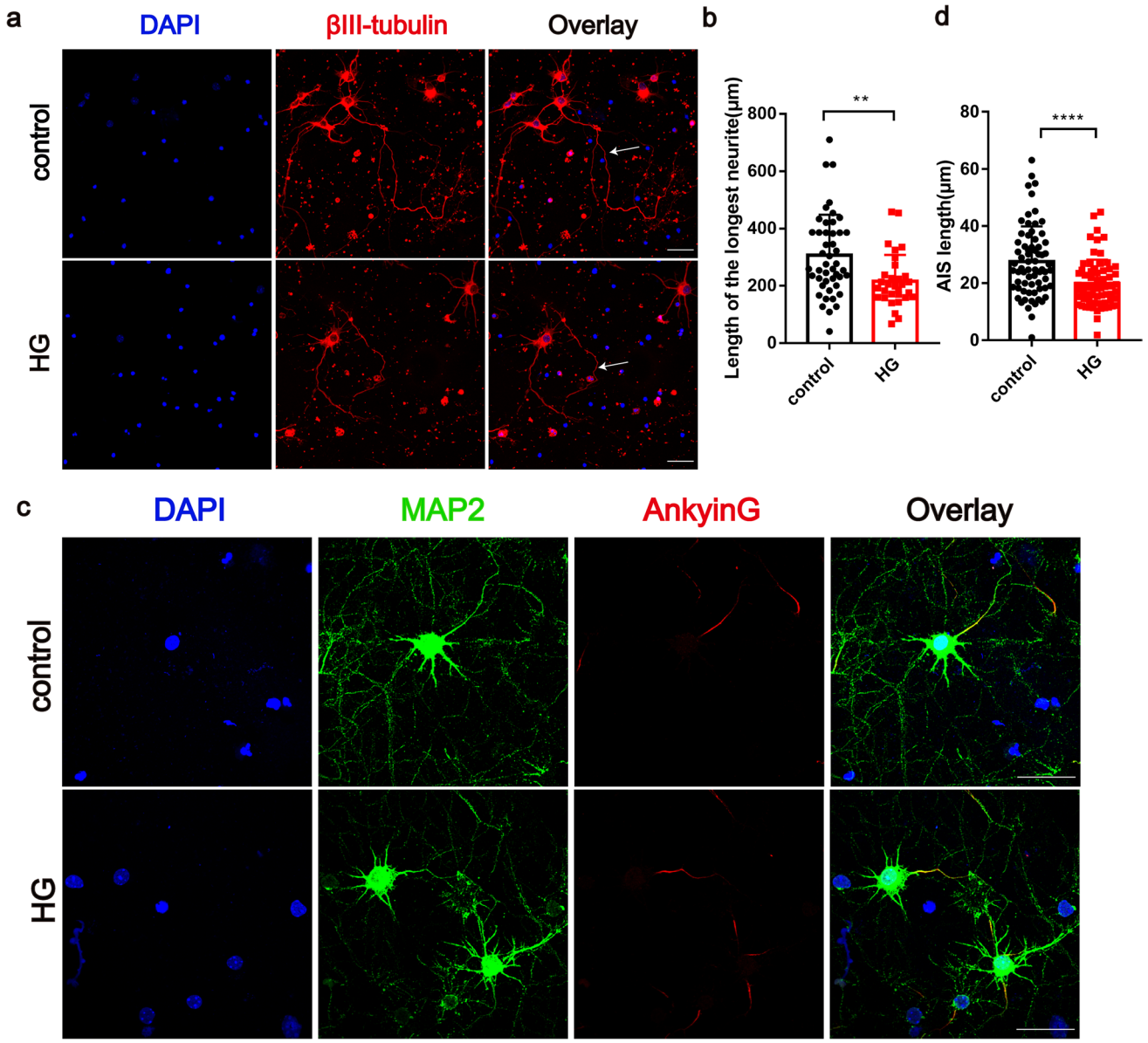

Fig. 3 Neurite outgrowth and axon initial segment in the primary neurons exposed to high glucose. **a**–**d** Representative immunofluorescence images for βIII-tubulin (**a**) or AnkyinG (**c**) with quantitative results of the longest neurite length (**b**) or AIS length (**d**) in primary hippocampal neurons treated with 900 mg/dl glucose or isotonic mannitol for 72 h. The arrow indicates the longest neurites. **b**: control, $n=46$; HG, $n=31$; **d**: control, $n=69$; HG, $n=67$ neurons from three independent experiments. $^{**}P<0.01$, $^{****}P<0.0001$ determined by Student *t*-test. Scale bar, 50 μm. Data represent means ± SD. βIII-tubulin, class III beta-tubulin; AIS, axon initial segment; MAP2, microtubule-associated protein 2; HG, high glucose

Next, we measured expression levels of synapse-related proteins including post- and pre-synaptic proteins. Western blot analysis revealed that postsynaptic protein PSD95 were significantly decreased in AAV-vector-treated db/db mice (fold change: 1.3 ± 0.1491), whereas PirB deficiency significantly restored levels of this proteins ($F_{(3,8)}=10.04$, one-way ANOVA; m/m + AAV-vector vs db/db + AAV-vector, $P=0.0110$; db/db + AAV-vector vs db/db + AAV-PirBi, $P=0.0052$; Fig. 5b, d). Although presynaptic protein synaptophysin (Syp) was comparable between diabetic mice and non-diabetic mice, PirB depletion significantly increased protein level of Syp in diabetic mice relative to the db/db + AAV-vector group ($F_{(3,8)}=9.206$, one-way ANOVA; db/db + AAV-vector vs db/db + AAV-PirBi, $P=0.0179$; Fig. 5c, e). Additionally, the protein level of Syp in PirB-deficient m/m mice was also slightly increased compared to m/m mice treated with AAV-vector (m/m + AAV-vector vs m/m + AAV-PirBi, $P=0.0401$; Fig. 5c, e). These results

were further confirmed by in situ staining of Syp (Fig. 5f) or PSD95 puncta (Online Resource 1) in hippocampal slices.

We next assessed neural morphology of pyramidal neurons using Golgi staining in m/m and db/db mice after stereotaxic injection. Sholl analysis revealed that compared with db/db + AAV-vector group, the sholl intersections were significantly more in pyramidal neurons of PirB-deficient db/db mice at a distance of 80–140 μm from soma to terminal ($F_{(3,2208)} = 135$, two-way ANOVA, post hoc analysis: db/db + AAV-vector vs db/db + AAV-PirBi; 80 μm, $P = 0.0263$; 90 μm, $P = 0.0008$; 100–110 μm, $P < 0.0001$; 120 μm, $P = 0.0002$; 130 μm, $P = 0.0021$; 140 μm, $P = 0.0078$; Fig. 6a–b) and the total dendrite length was also increased ($F_{(3,70)} = 12.48$, one-way ANOVA, db/db + AAV-vector vs db/db + AAV-PirBi: $P = 0.0282$; Fig. 6c), indicating that PirB knockdown in hippocampus restored decreased dendrite branching in diabetic brains. Additionally, the sholl intersections at a distance of 140–180 μm (m/m + AAV-vector vs m/m + AAV-PirBi: 140 μm, $P = 0.0329$; 150 μm, $P = 0.0031$; 160 μm, $P = 0.0244$; 170 μm, $P = 0.0048$; 180 μm, $P = 0.0122$) in m/m + AAV-PirBi group were slightly greater than m/m + AAV-vector group, suggesting that PirB knockdown also mildly enhanced dendrite complexity in m/m mice (Fig. 6b–c). We also found that spine density of pyramidal neurons was increased in PirB-deficient db/db mice relative to db/db + AAV-vector group ($F_{(3,44)} = 19.68$, one-way ANOVA, db/db + AAV-vector vs db/db + AAV-PirBi: $P < 0.0001$), similar benefits of PirB deficiency were also found in non-diabetic mice even there were not statistical significance (m/m + AAV-vector vs m/m + AAV-PirBi: $P = 0.1878$) (Fig. 6d–e). These data demonstrate that PirB down-regulation rescues synapse-related proteins loss and dendritic morphology defects in diabetic brains.

PirB Depletion Facilitated Recovery of Cognitive Dysfunction in db/db Mice

To further determine whether PirB deficiency affords a protective effect on diabetes-induced cognitive decline, we evaluated the learning and memory performance of the different groups of mice at the age of 24 weeks with the MWM paradigm (Fig. 7a). While in non-diabetic mice, the time required to locate the hidden platform was still significantly shorter than diabetic mice ($F_{(3,130)} = 26.48$, two-way ANOVA, m/m + AAV-vector vs db/db + AAV-vector: day 3, $P = 0.0086$; day 4, $P = 0.0012$; day 5, $P = 0.0095$; Fig. 7b), AAV-PirBi-treated db/db mice tended to require less time to locate the platform compared to the AAV-vector-treated groups of mice (Fig. 7b). Similar results were also observed in path efficiency ($F_{(3,128)} = 6.999$, two-way ANOVA, m/m + AAV-vector vs db/db + AAV-vector: day 5, $P = 0.0079$; Fig. 7c). Upon removal of the platform, db/db mice treated with AAV-PirBi performed significantly better to retain spatial memory compared to the AAV-vector treated groups of db/db mice ($F_{(3,28)} = 3.609$, one-way ANOVA, m/m + AAV-vector vs db/db + AAV-vector: $P = 0.0440$, db/db + AAV-vector vs db/db + AAV-PirBi: $P = 0.0397$). In addition, there was comparable performance between m/m + AAV-PirBi and m/m + AAV-vector groups ($P > 0.05$; Fig. 7b–f), indicating that knockdown PirB in m/m mice was not sufficient to enhance cognitive function even though positive effects were observed in neural morphology and biochemical analysis. Collectively, these results provided evidence that knockdown PirB mitigated diabetes-related cognitive decline.

Discussion

Our study identified PirB as a key player in negative effects on hippocampal neuroplasticity from diabetes. We found PirB expression upregulation in primary neurons exposed to high glucose and the hippocampus of 24-week-old db/db mice. Notably, RNAi-mediated reduction in PirB function resulted in robustly extend process of high glucose-treated primary neurons, highlighting the repression effect of PirB on axon outgrowth. Of note, PirB depletion in the hippocampus rescued decreased dendritic branching and spines density of diabetic brains and even improved cognitive deficits in 24-week-old db/db mice. This study verifies a novel role of PirB and provides a potential target for diabetes-associated cognitive dysfunction therapy.

There is a well-established association between diabetes and cognitive dysfunction based on substantial epidemiological studies [3, 25, 26]. Despite accumulating evidences also supported that db/db mice have cognitive dysfunction phenotype, the age of the animal model varies between studies [10, 24, 27]. Several age groups of cognitive function were assessed by our laboratories (unpublished data) and other study [27], showing that 4 weeks db/db mice displayed preserved cognitive function, and 8 or 14 weeks db/db mice developed very limited dysfunction, whereas 24 or 26 week db/db mice showed significant learning and memory impairment. In the present study, we chose 24-week-old db/db mice as our experimental model and confirmed that it displayed an impaired performance in the MWM task, which is a valid indicator of hippocampal-dependent spatial memory. Following these observations, it seems that db/db mice show age-dependent memory disturbance, which is in accordance with clinical findings that the prevalence of mild cognitive impairment and dementia rises substantially with increasing age in the general population including type 2 diabetes patients [28, 29]. Apart from aging as a critical driver for brain damage, hyperglycemia may well be another major contributor, which can be detected as early as 4 weeks of

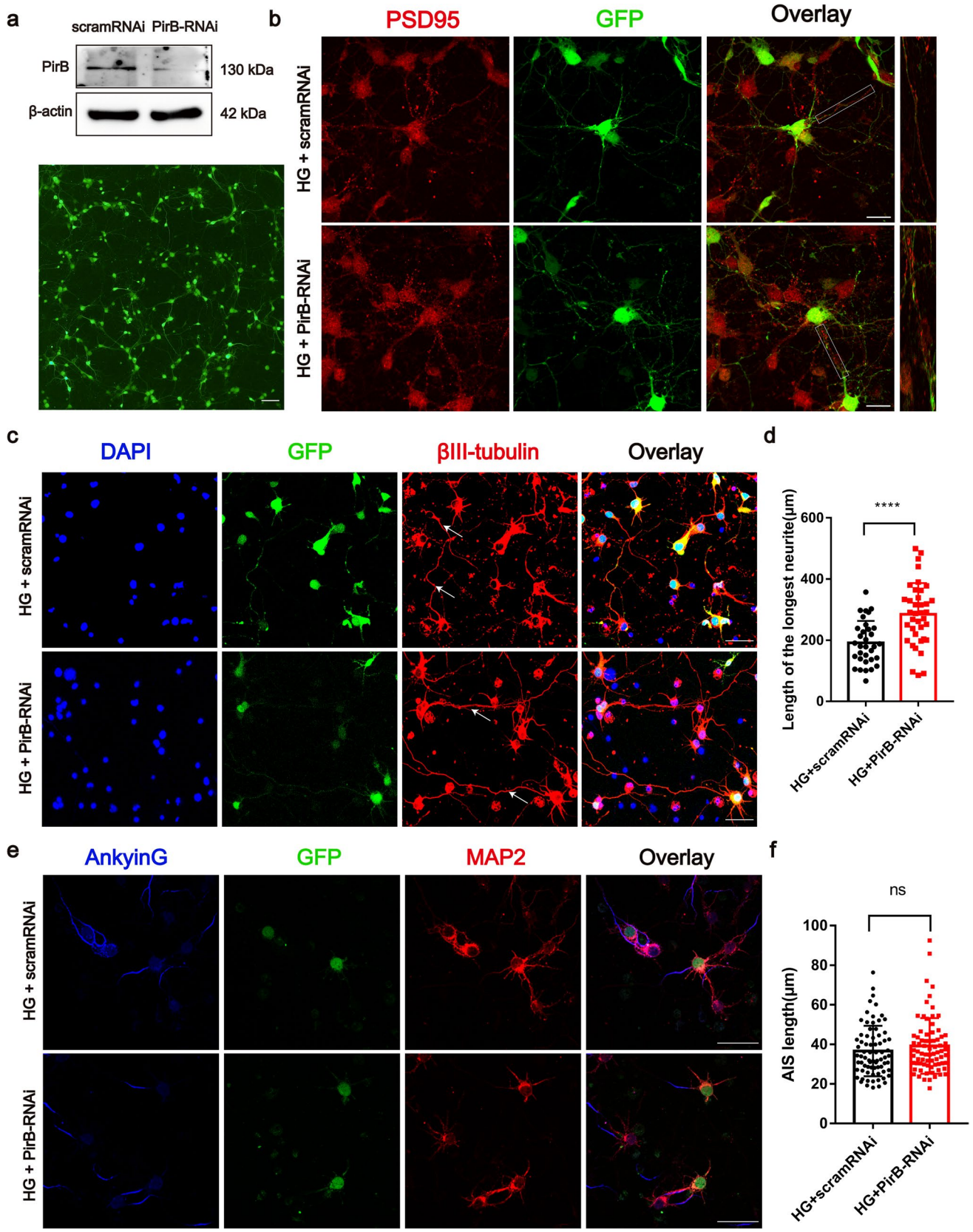
a
scramRNAi PirB-RNAi
PirB
130 kDa
β-actin
42 kDa
b
PSD95
GFP
Overlay
HG + scramRNAi
HG + PirB-RNAi
c
DAPI
GFP
βIII-tubulin
Overlay
HG + scramRNAi
HG + PirB-RNAi
d
Length of the longest neurite(μm)
****
600
400
200
0
HG+scramRNAi
HG+PirB-RNAi
e
AnkyinG
GFP
MAP2
Overlay
HG + scramRNAi
HG + PirB-RNAi
f
AIS length(μm)
ns
100
80
60
40
20
0
HG+scramRNAi
HG+PirB-RNAi

◂**Fig. 4** Effect of PirB knockdown on neurite outgrowth in the primary neurons exposed to high glucose. **a** Infection efficiency was confirmed by western blotting and immunofluorescence assay 72 h after the transfection. Scale bar, 50 μm. **b** Representative immunofluorescence images for PSD95 in primary hippocampal neurons treated with 900 mg/dl glucose or isotonic mannitol for 72 h after transfection of PirB-RNAi or scramRNAi. Data were collected from three independent experiments. Scale bar, 25 μm. **c–f** Representative immunofluorescence images for βIII-tubulin (**c**) or AnkyinG (**e**) with quantitative results of the longest neurite length (**d**) or AIS length (**f**) in primary hippocampal neurons treated with 900 mg/dl glucose or isotonic mannitol for 72 h after transfection of PirB-RNAi or scramRNAi. The arrow indicates the longest neurites. **d**: HG + scramRNAi, $n = 33$; HG + PirB-RNAi, $n = 38$; **f**: HG + scramRNAi, $n = 74$; HG + PirB-RNAi, $n = 74$ neurons from three independent experiments. $^{****}P < 0.0001$ determined by Student *t*-test. Scale bar, **c** and **e**, 50 μm. Data represent means ± SD. PirB, Paired immunoglobulin-like receptor B; PSD95, Postsynaptic density protein 95; HG, high glucose; βIII-tubulin, class III beta-tubulin; MAP2, microtubule-associated protein 2; AIS, axon initial segment; GFP, green fluorescent protein

age in db/db mice, and glucose levels continue to increase until maintain > 400 mg/dl for the rest long time. Since brain is almost entirely dependent on glucose for its energy and neurotransmission, aging brain seems to become much more susceptible to cellular damage induced by chronically elevated glucose levels, which could explain the occurrence of severe cognitive dysfunction primarily in older diabetes patients (> 65 years of age) and aging db/db mice [1, 3]. Of course, other risk factors, such as insulin resistance and dyslipidemia, may also be involved in this process. Overall, our findings provide evidence that 24-week-old db/db mice develop significant cognitive dysfunction.

Neural plasticity refers to the ability of the brain to adapt, change, and reorganize throughout life. Numerous studies have provided evidence that diabetes negatively affects neural plasticity, including dendrites contraction, spines loss, impaired neurogenesis, and synaptic efficacy, which may contribute to cognitive decline in diabetes [9, 30]. However, the precise mechanisms underlying those developments have not yet been addressed. PirB, a receptor mainly expressed in neurons, is an important inhibitor for nervous system plasticity [13, 14, 31]. In this study, we identified PirB protein elevation and axon growth markers GAP43 expression downregulation in the hippocampus of db/db mice. Similar results were also found in primary hippocampal neurons exposed to high glucose, accompanied by axon outgrowth restriction, which indicated that high glucose triggers PirB-dependent axon outgrowth inhibition. The average length of the longest neurite in RNAi-depleted neurons was increased relative to control, as expected if PirB limits axon outgrowth in a high glucose environment. These results are consistent with previous studies demonstrating PirB expression was induced in multiple pathological conditions including hypoxic-ischemic brain damage, spinal cord injury, and retinopathy and was required for the inhibition of neurite outgrowth [14, 20, 32, 33]. Our findings verify the crucial role of PirB in high glucose-induced axon outgrowth inhibition, expanding the involvement of its known pathological conditions.

The AIS is a specialized functional domain that sits at the base of axons, which generates and shapes action potential before that are propagated along the axon [34]. Recent studies have identified that disruption of the AIS is a key pathophysiological event in various neurological and psychiatric disorders, such as epilepsy, schizophrenia, and AD [35–37]. Our present data showed that AIS length was shorter in primary hippocampal neurons cultured high glucose condition, which is consistent with the findings of a previous study in db/db mice that reported AIS shortening in both prefrontal cortex and hippocampus [23, 24]. However, blocking PirB function failed to reverse AIS shortening. The reasons may come from the following points: First, PirB as an endogenous inhibitor of neurite regeneration seems to mainly act on the distal axon terminal, resulting in actin depolymerization, growth cone collapse, and neurite retraction. While the AIS is positioned in the proximal axon, a unique neuronal compartment with distinct molecular organization characterized by enrichment for voltage-gated sodium channels and a unique repertoire of sub-membranous cytoskeletal scaffolds [38]. According to previous study, AIS shortening occurred at 10 weeks of age of db/db mice in the absence of changes in the morphological appearance of the medial prefrontal cortex or hippocampus, or in expression levels of neuronal and myelin proteins [23]. It seems that the AIS shortening might be caused by other factors, not PirB-mediated neurite regeneration inhibition following nerve injury. While the molecular and cellular mechanisms of structural AIS alteration are largely unknown, many previous studies consistently point to the regulation of intracellular calcium levels and calcium-dependent enzymes play a crucial role in this process [39, 40]. Second, adaptive changes to the location and length of the AIS are also one of the forms of AIS plasticity which can fine-tune neuronal excitability for optimal function in response to activity [41]. It remains unknown that whether such AIS shortening is a pathological change caused by type 2 diabetes, or adaptive change to maintain neural circuit activities which refers to the regulation of a sophisticated network. An inverse correlation between AIS length and blood glucose was observed based on previous study and AIS shortening does not occur if hyperglycemia is controlled [23], which is consistent with our results that reduced length of the AIS was observed in high glucose medium. It seems that hyperglycemia is the primary cause of AIS shortening. Future studies are required to identify the key mechanism of diabetes-related AIS changes.

Dendritic remodeling as another form of neuroplasticity is also affected by diabetes, manifested by decreased dendritic branching and spines density in both type 1 and type 2

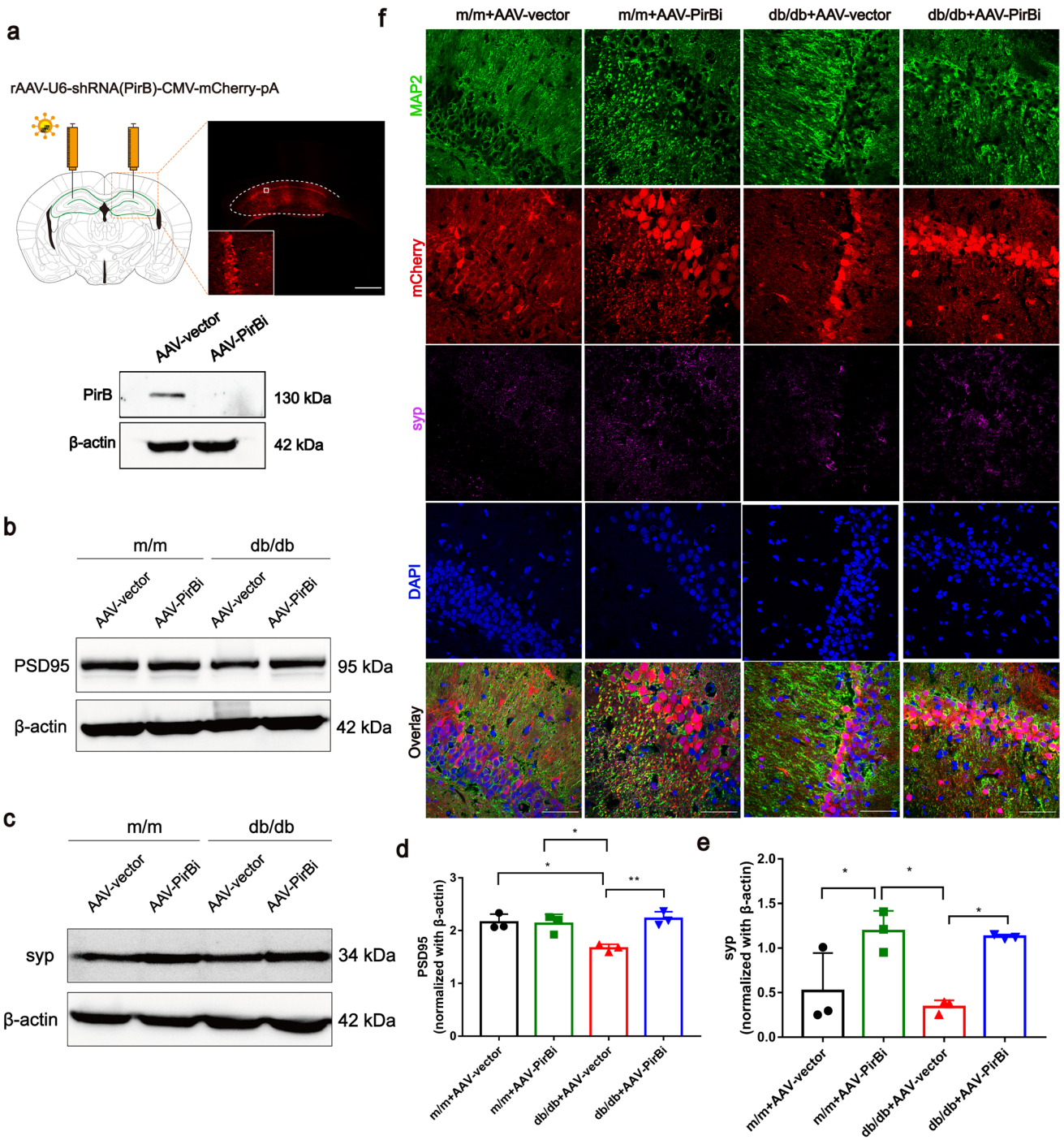

Fig. 5 Effect of PirB knockdown on synapse-related proteins in the hippocampus of db/db mice. **a** Transfection efficiency was confirmed by western blot and immunofluorescence assay. Scale bar, 500 μm. **b**–**e** Western blot of PSD95 (**b**) or Syp (**c**) and quantitative results (**d**–**e**) in the hippocampus of experimental mice treated with AAV-PirBi or AAV-vector. $n = 3$. $^{*}P < 0.05$, $^{**}P < 0.01$ determined by one-way ANOVA with Tukey's multiple comparisons tests. **f** Representative images of immunofluorescence for Syp and MAP2 on the dendrites of pyramid neurons. Scale bar, 50 μm. Data represent means ± SD. PSD95, Postsynaptic density protein 95; Syp, Synaptophysin; PirB, Paired immunoglobulin-like receptor B; AAV, Adeno-associated virus; MAP2, microtubule-associated protein 2

diabetes models [9]. Our study revealed that PirB depletion rescued dendritic morphology defects in db/db mice. Further benefits were also found in behavioral tests. These results are in line with previous studies demonstrating increased synaptic plasticity, indicated by elevated synapses frequency, higher spine density, and greater electrophysiological

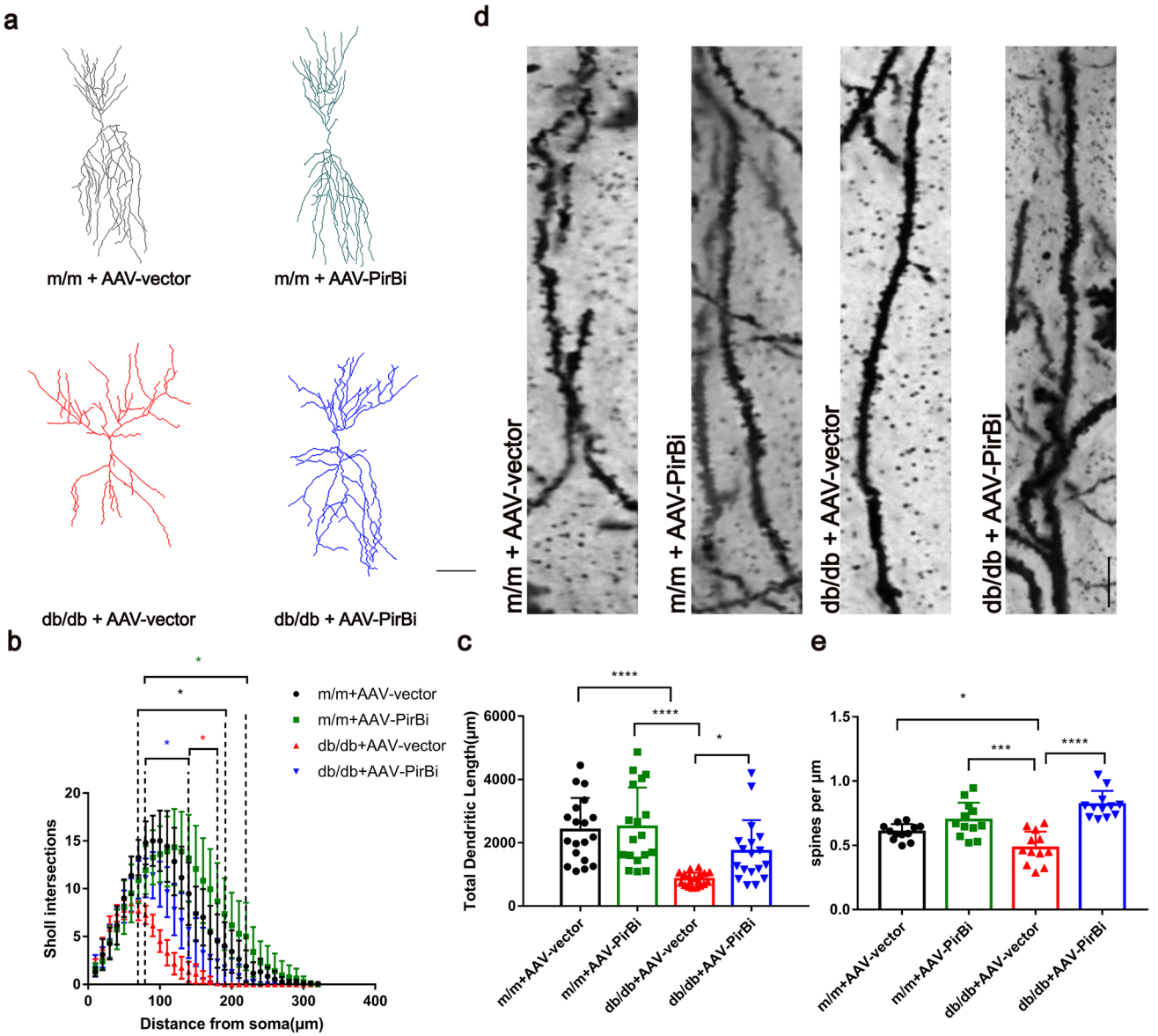

Fig. 6 Effect of PirB knockdown on dendritic morphology of pyramidal neurons in hippocampus of db/db mice. **a** Representative neurons from four groups following Golgi staining and sholl analysis. Scale bar, 50 μm. **b** Dendritic complexity shown by the number of dendritic intersections plotted against the distance from the soma in the hippocampal neurons of experimental mice treated with AAV-PirBi and AAV-vector. m/m + AAV-vector, $n = 19$; m/m + AAV-PirBi, $n = 18$; db/db + AAV-vector, $n = 19$; db/db + AAV-PirBi, $n = 18$. The different colors of asterisk show varies with the range of statistical significance determined by two-way ANOVA with Tukey' multiple comparisons test. *(black): db/db + AAV-vector vs m/m + AAV-vector. *(blue): db/db + AAV-vector vs db/db + AAV-PirBi. *(green): db/db + AAV-vector vs m/m + AAV-PirBi. *(red): m/m + AAV-vector vs m/m + AAV-PirBi. **c** Total dendritic length for pyramidal neurons in the hippocampus of experimental mice. m/m + AAV-vector, $n = 19$; m/m + AAV-PirBi, $n = 18$; db/db + AAV-vector, $n = 19$; db/db + AAV-PirBi, $n = 18$. $^{*}P < 0.05$, $^{****}P < 0.0001$ determined by one-way ANOVA with Tukey's multiple comparisons test. **d**–**e** Representative images of Golgi-stained dendritic segments (**d**) and quantification of the dendritic spine density (**e**) on pyramidal neurons dendrites in the hippocampus of db/db and m/m mice treated with AAV-PirBi or AAV-vector. $n = 12$/group. $^{*}P < 0.05$, $^{****}P < 0.0001$ determined by one-way ANOVA with Tukey's multiple comparisons test. Scale bar, 10 μm. All measurements were from three mice each. **b**: Data represent means + 95% confidence interval; **c** and **e**: Data represent means ± SD

properties accompanied by improved behavior performance when PirB was depleted in the visual cortex or hippocampus [15, 16, 18, 19]. Of note, non-diabetic mice in our study also benefited from PirB silence in the hippocampus, manifesting slightly enhanced synapse-related proteins expression, sholl interactions, and spine density despite not all these indicators have statistical significance. It is reasonable that the role of PirB in the healthy brain has been explored in one study,

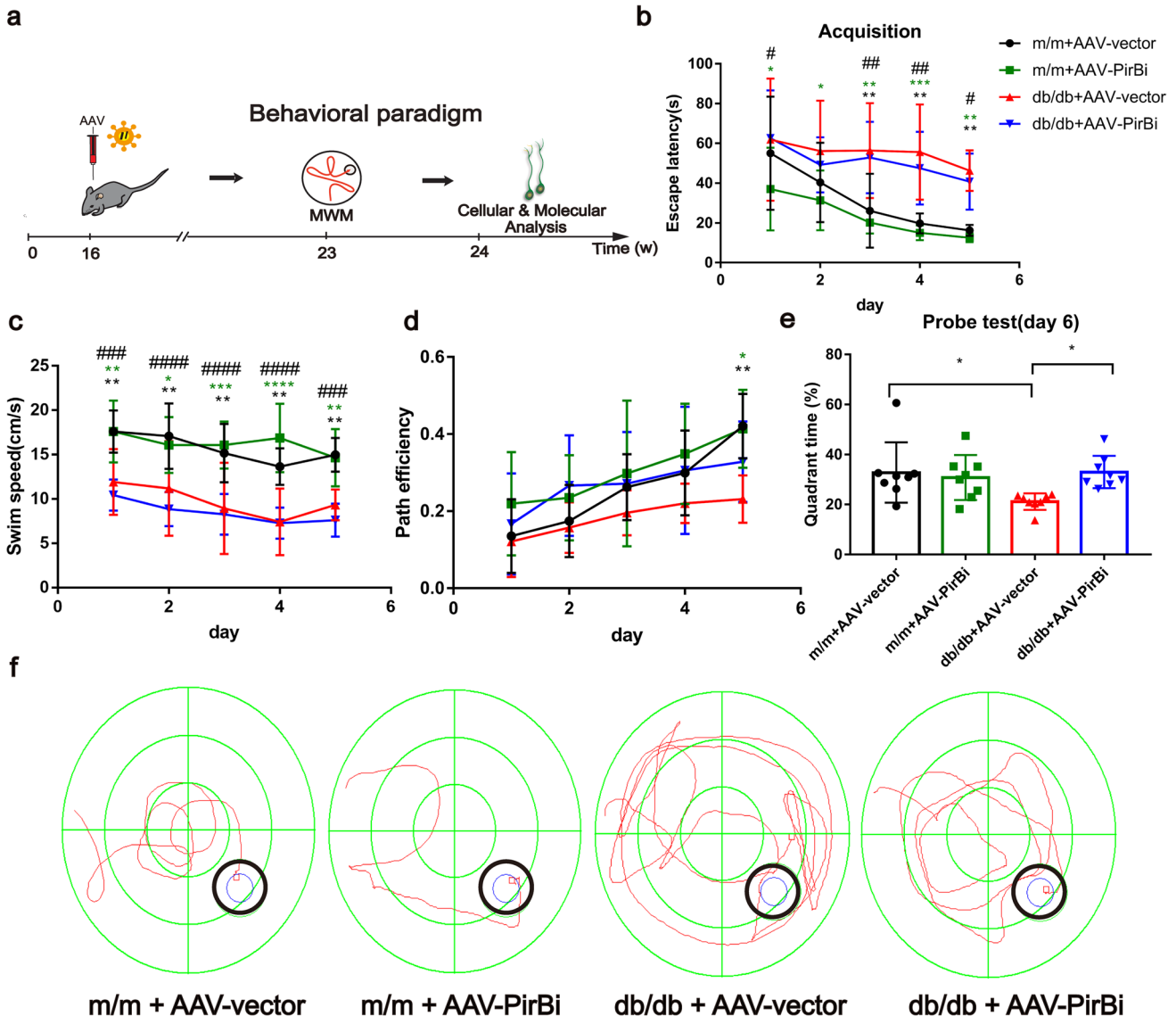

Fig. 7 Effect of PirB knockdown on the cognitive function of db/db mice. **a** Experimental timeline. Db/db and m/m mice were injected bilaterally with AAV-PirBi or AAV-vector prior to 2 months of behavioral testing. **b**–**e** Results of MWM test in db/db and m/m mice treated with AAV-PirBi and AAV-vector. Escape latency (**b**), swim speed (**c**), and path efficiency (**d**) in the training session of the MWM test. **e** Time in the target quadrant during the probe trial on the last day of the MWM test. $n = 7$–8/group. For **b**–**d**, $^{*}P < 0.05$, $^{**}P < 0.01$, $^{***}P < 0.001$, $^{****}P < 0.0001$, $^{\#}P < 0.05$, $^{\#\#}P < 0.01$, $^{\#\#\#}P < 0.001$, $^{\#\#\#\#}P < 0.0001$ determined by two-way ANOVA with Tukey's multiple comparisons test. *(black): db/db + AAV-vector vs m/m + AAV-vector. *(green): db/db + AAV-vector vs m/m + AAV-PirBi. #: m/m + AAV-PirBi vs db/db + AAV-PirBi. For **e**, $^{*}P < 0.05$ determined by one-way ANOVA with Tukey's multiple comparisons test. **f** Representative traces of experimental mice treated with AAV-PirBi or AAV-vector in MWM test. Data represent means ± SD

which showed deficient LTD and increased LTP in PirB-deficient hippocampal slices accompanied by better learning and memory of PirB null mice [18], whereas we did not observe the enhanced behavioral performance of PirB-deficient m/m mice in our research. This discrepancy may be attributed to different mice strains, ages, and behavioral paradigms used in the two studies.

Despite the well-described function of PirB in the repression of axon growth and synaptic plasticity, the precise mechanisms have not been completely elucidated. Nevertheless, several supposed pathways exist based on some evidence. POSH has been proven to act as a key intracellular signal-transduction molecule downstream of Nogo66 and PirB in relaying process outgrowth inhibition. Downstream of POSH, LZK/JNK/MKK, and Shroom3/ROCK signaling pathway independently modulate neurite outgrowth, which both result in the myosin IIA activation and neurite growth inhibition [13, 14, 42]. In this study,

we identified that POSH was elevated in the hippocampus of db/db mice, indicating that PirB may inhibit axon outgrowth in a POSH-dependent mechanism, but the identity of POSH in this pathway remains to be determined. Another supposed PirB-dependent signaling pathway regarding recruitment of SHP-1/SHP-2 after ligands bind to the extracellular domain of PirB subsequently leads to the dephosphorylation of the TrkB, PI3K, and Akt activation, and ultimately causing actin depolymerization and axon inhibition [43–45]. Considering the dysregulation of the PI3K-Akt-mTOR pathway exists in diabetic brains, it is reasonable to believe that both signaling pathways may participate in PirB-mediated neural plasticity changes.

Given that PirB serves as a well-established role in the repression of neural plasticity, targeting PirB may be a promising candidate intervention for CNS injury. Currently, drug agents targeting PirB ectodomain have been explored in this field. For example, a soluble PirB ectodomain was generated to block PirB interaction with endogenous ligands and was demonstrated to enable significant functional and structural recovery from amblyopia [15]. Another recombinant fusion protein, transactivator of transcription-PirB extracellular peptide, that can cross the blood–brain barrier, was produced later and was proven to improve long-term neurological deficits after stroke [20]. Other similar agents, including a novel PirB antagonist peptide PAP11 and a double-targeted granulocyte–macrophage colony-stimulating factor-NgR-PirB nucleic acid vaccine, were constructed to exert neuroprotective effects as well [46, 47]. Thus, it is more interesting to verify whether these available agents would also ameliorate cognitive dysfunction in db/db mice.

Nevertheless, there are several limitations to consider in our study. First, as mentioned by others [24, 27], 24-week-old db/db mice used in our study displayed decreased locomotor activity, which might mask other possible abnormal behaviors that existed in this model since locomotor activity is an essential factor affecting the outcomes of most behavioral tests. Future studies should include other types of animal models, such as high-fat-diet feeding with a subsequent injection of a low dose of streptozotocin. Second, it is well-known that neural structural and functional plasticity are likely tightly linked [48]. Our present study only focuses on neural structural plasticity, whether such alterations in neural morphology are accompanied by functional changes remains to be identified in our next work.

In summary, our results provide novel insights into the mechanisms of altered neural structural plasticity affected by diabetes, highlighting the detrimental role of PirB in axon outgrowth and dendritic remodeling. This study may offer a novel target for the treatment of diabetes-associated cognitive decline and neurodegeneration.

Supplementary Information The online version contains supplementary material available at https://doi.org/10.1007/s12035-021-02679-1.

Acknowledgements The authors gratefully acknowledge Xiaoli Qu from the State Key Laboratory for Manufacturing Systems Engineering of Xi'an Jiaotong University for her help on image acquisition.

Author Contribution Q.W., Q.Z., and K.R.P. conceptualized the study. K.R.P. and Q.Z. designed experiments and drafted the manuscript. K.R.P. performed experiments. M.Y.W., Y.X.Z., M.Y., and J.Y.S. assisted with experimental and execution. J.T. and H.L.M. were involved in data analysis. All authors read and approved the final manuscript.

Funding This work was supported by the National Natural Science Foundation of China (Nos. 81774113, 81974540, 81901237), Beijing, China.

National Natural Science Foundation of China,81774113,Qiang Wang,81974540,Qiang Wang,81901237,Qian Zhai

Availability of Data and Material The datasets generated during and/or analyzed during the current study are available from the corresponding author on reasonable request.

Code availability (Software Application or Custom Code) GraphPad Prism Version 8.0; Image J Version 1.51 J.

Declarations

Ethics approval Efforts were made to minimize animal suffering and to reduce the number of animals used. All animal experiments were approved by the Institutional Animal Care and Use Committees of Xi'an Jiaotong University (Xi'an, China; 2019–060) in accordance with the National Institutes of Health guidelines.

Consent to Participate Not applicable.

Consent for Publication Not applicable.

Competing Interests The authors declare no competing interests.

References

1. Srikanth V, Sinclair AJ, Hill-Briggs F, Moran C, Biessels GJ (2020) Type 2 diabetes and cognitive dysfunction—towards effective management of both comorbidities. Lancet Diabetes Endocrinol 8(6):535–545. https://doi.org/10.1016/s2213-8587(20)30118-2
2. Pearson-Stuttard J, Bennett J, Cheng YJ, Vamos EP, Cross AJ, Ezzati M, Gregg EW (2021) Trends in predominant causes of death in individuals with and without diabetes in England from 2001 to 2018: an epidemiological analysis of linked primary care records. Lancet Diabetes Endocrinol 9(3):165–173. https://doi.org/10.1016/s2213-8587(20)30431-9
3. Biessels GJ, Despa F (2018) Cognitive decline and dementia in diabetes mellitus: mechanisms and clinical implications. Nat Rev Endocrinol 14(10):591–604. https://doi.org/10.1038/s41574-018-0048-7
4. Cho NH, Shaw JE, Karuranga S, Huang Y, da Rocha Fernandes JD, Ohlrogge AW, Malanda B (2018) IDF Diabetes Atlas: global estimates of diabetes prevalence for 2017 and projections for

2045. Diabetes Res Clin Pract 138:271–281. https://doi.org/10.1016/j.diabres.2018.02.023
5. Bae JR, Kim SH (2017) Synapses in neurodegenerative diseases. BMB Rep 50(5):237–246. https://doi.org/10.5483/bmbrep.2017.50.5.038
6. Burke SN, Barnes CA (2006) Neural plasticity in the ageing brain. Nat Rev Neurosci 7(1):30–40. https://doi.org/10.1038/nrn1809
7. Stranahan AM, Lee K, Martin B, Maudsley S, Golden E, Cutler RG, Mattson MP (2009) Voluntary exercise and caloric restriction enhance hippocampal dendritic spine density and BDNF levels in diabetic mice. Hippocampus 19(10):951–961. https://doi.org/10.1002/hipo.20577
8. Chen J, Liang L, Zhan L, Zhou Y, Zheng L, Sun X, Gong J, Sui H, Jiang R, Zhang F, Zhang L (2014) ZiBuPiYin recipe protects db/db mice from diabetes-associated cognitive decline through improving multiple pathological changes. PLoS ONE 9(3):e91680. https://doi.org/10.1371/journal.pone.0091680
9. Ho N, Sommers MS, Lucki I (2013) Effects of diabetes on hippocampal neurogenesis: links to cognition and depression. Neurosci Biobehav Rev 37(8):1346–1362. https://doi.org/10.1016/j.neubiorev.2013.03.010
10. Stranahan AM, Arumugam TV, Cutler RG, Lee K, Egan JM, Mattson MP (2008) Diabetes impairs hippocampal function through glucocorticoid-mediated effects on new and mature neurons. Nat Neurosci 11(3):309–317. https://doi.org/10.1038/nn2055
11. Gispen WH, Biessels GJ (2000) Cognition and synaptic plasticity in diabetes mellitus. Trends Neurosci 23(11):542–549. https://doi.org/10.1016/s0166-2236(00)01656-8
12. Li X-L, Aou S, Oomura Y, Hori N, Fukunaga K, Hori T (2002) Impairment of long-term potentiation and spatial memory in leptin receptor deficient rodents. Neuroscience 113(3):607–615. https://doi.org/10.1016/s0306-4522(02)00162-8
13. Gou Z, Mi Y, Jiang F, Deng B, Yang J, Gou X (2014) PirB is a novel potential therapeutic target for enhancing axonal regeneration and synaptic plasticity following CNS injury in mammals. J Drug Target 22(5):365–371. https://doi.org/10.3109/1061186X.2013.878939
14. Liu J, Wang Y, Fu W (2015) Axon regeneration impediment: the role of paired immunoglobulin-like receptor B. Neural Regen Res 10(8):1338–1342. https://doi.org/10.4103/1673-5374.162771
15. Bochner DN, Sapp RW, Adelson JD, Zhang S, Lee H, Djurisic M, Syken J, Dan Y, Shatz CJ (2014) Blocking PirB up-regulates spines and functional synapses to unlock visual cortical plasticity and facilitate recovery from amblyopia. Science Translational Medicine 6(258):258ra140. https://doi.org/10.1126/scitranslmed.3010157
16. Djurisic M, Vidal GS, Mann M, Aharon A, Kim T, Ferrao Santos A, Zuo Y, Hubener M, Shatz CJ (2013) PirB regulates a structural substrate for cortical plasticity. Proc Natl Acad Sci U S A 110(51):20771–20776. https://doi.org/10.1073/pnas.1321092110
17. Vidal GS, Djurisic M, Brown K, Sapp RW, Shatz CJ (2016) Cell-autonomous regulation of dendritic spine density by PirB. eNeuro 3 (5):ENEURO.0089-0016.2016. https://doi.org/10.1523/ENEURO.0089-16.2016
18. Djurisic M, Brott BK, Saw NL, Shamloo M, Shatz CJ (2019) Activity-dependent modulation of hippocampal synaptic plasticity via PirB and endocannabinoids. Mol Psychiatry 24(8):1206–1219. https://doi.org/10.1038/s41380-018-0034-4
19. Kim T, Vidal GS, Djurisic M, Williams CM, Birnbaum ME, Garcia KC, Hyman BT, Shatz CJ (2013) Human LilrB2 is a β-amyloid receptor and its murine homolog PirB regulates synaptic plasticity in an Alzheimer's model. Science 341(6152):1399–1404. https://doi.org/10.1126/science.1242077
20. Deng B, Li L, Gou X, Xu H, Zhao Z, Wang Q, Xu L (2018) TAT-PEP enhanced neurobehavioral functional recovery by facilitating axonal regeneration and corticospinal tract projection after stroke. Mol Neurobiol 55(1):652–667. https://doi.org/10.1007/s12035-016-0301-9
21. Deng B, Bai F, Zhou H, Zhou D, Ma Z, Xiong L, Wang Q (2016) Electroacupuncture enhances rehabilitation through miR-181b targeting PirB after ischemic stroke. Scientific Reports 6:38997. https://doi.org/10.1038/srep38997
22. Zhao ZH, Deng B, Xu H, Zhang JF, Mi YJ, Meng XZ, Gou XC, Xu LX (2017) PirB overexpression exacerbates neuronal apoptosis by inhibiting TrkB and mTOR phosphorylation after oxygen and glucose deprivation injury. Cell Mol Neurobiol 37(4):707–715. https://doi.org/10.1007/s10571-016-0406-8
23. Yermakov LM, Drouet DE, Griggs RB, Elased KM, Susuki K (2018) Type 2 diabetes leads to axon initial segment shortening in db/db mice. Front Cell Neurosci 12:146. https://doi.org/10.3389/fncel.2018.00146
24. Yermakov LM, Griggs RB, Drouet DE, Sugimoto C, Williams MT, Vorhees CV, Susuki K (2019) Impairment of cognitive flexibility in type 2 diabetic db/db mice. Behav Brain Res 371:111978. https://doi.org/10.1016/j.bbr.2019.111978
25. McCrimmon RJ, Ryan CM, Frier BM (2012) Diabetes and cognitive dysfunction. Lancet 379(9833):2291–2299. https://doi.org/10.1016/s0140-6736(12)60360-2
26. Ryan CM, van Duinkerken E, Rosano C (2016) Neurocognitive consequences of diabetes. Am Psychol 71(7):563–576. https://doi.org/10.1037/a0040455
27. Ramos-Rodriguez JJ, Ortiz O, Jimenez-Palomares M, Kay KR, Berrocoso E, Murillo-Carretero MI, Perdomo G, Spires-Jones T, Cozar-Castellano I, Lechuga-Sancho AM, Garcia-Alloza M (2013) Differential central pathology and cognitive impairment in pre-diabetic and diabetic mice. Psychoneuroendocrinology 38(11):2462–2475. https://doi.org/10.1016/j.psyneuen.2013.05.010
28. Exalto LG, Biessels GJ, Karter AJ, Huang ES, Katon WJ, Minkoff JR, Whitmer RA (2013) Risk score for prediction of 10 year dementia risk in individuals with type 2 diabetes: a cohort study. Lancet Diabetes Endocrinol 1(3):183–190. https://doi.org/10.1016/s2213-8587(13)70048-2
29. Nichols E, Szoeke CEI, Vollset SE, Abbasi N, Abd-Allah F, Abdela J, Aichour MTE, Akinyemi RO, Alahdab F, Asgedom SW, Awasthi A, Barker-Collo SL, Baune BT, Béjot Y, Belachew AB, Bennett DA, Biadgo B, Bijani A, Bin Sayeed MS, Brayne C, Carpenter DO, Carvalho F, Catalá-López F, Cerin E, Choi J-YJ, Dang AK, Degefa MG, Djalalinia S, Dubey M, Duken EE, Edvardsson D, Endres M, Eskandarieh S, Faro A, Farzadfar F, Fereshtehnejad S-M, Fernandes E, Filip I, Fischer F, Gebre AK, Geremew D, Ghasemi-Kasman M, Gnedovskaya EV, Gupta R, Hachinski V, Hagos TB, Hamidi S, Hankey GJ, Haro JM, Hay SI, Irvani SSN, Jha RP, Jonas JB, Kalani R, Karch A, Kasaeian A, Khader YS, Khalil IA, Khan EA, Khanna T, Khoja TAM, Khubchandani J, Kisa A, Kissimova-Skarbek K, Kivimäki M, Koyanagi A, Krohn KJ, Logroscino G, Lorkowski S, Majdan M, Malekzadeh R, März W, Massano J, Mengistu G, Meretoja A, Mohammadi M, Mohammadi-Khanaposhtani M, Mokdad AH, Mondello S, Moradi G, Nagel G, Naghavi M, Naik G, Nguyen LH, Nguyen TH, Nirayo YL, Nixon MR, Ofori-Asenso R, Ogbo FA, Olagunju AT, Owolabi MO, Panda-Jonas S, Passos VMdA, Pereira DM, Pinilla-Monsalve GD, Piradov MA, Pond CD, Poustchi H, Qorbani M, Radfar A, Reiner RC, Robinson SR, Roshandel G, Rostami A, Russ TC, Sachdev PS, Safari H, Safiri S, Sahathevan R, Salimi Y, Satpathy M, Sawhney M, Saylan M, Sepanlou SG, Shafieesabet A, Shaikh MA, Sahraian MA, Shigematsu M, Shiri R, Shiue I, Silva JP, Smith M, Sobhani S, Stein DJ, Tabarés-Seisdedos R, Tovani-Palone MR, Tran BX, Tran TT, Tsegay AT, Ullah I, Venketasubramanian N, Vlassov V, Wang Y-P, Weiss J, Westerman R, Wijeratne T, Wyper GMA, Yano Y, Yimer EM,

Yonemoto N, Yousefifard M, Zaidi Z, Zare Z, Vos T, Feigin VL, Murray CJL (2019) Global, regional, and national burden of Alzheimer's disease and other dementias, 1990–2016: a systematic analysis for the Global Burden of Disease Study 2016. The Lancet Neurology 18(1):88–106. https://doi.org/10.1016/s1474-4422(18)30403-4

30. Xiong Y, Zhang S, Shi J, Fan Y, Zhang Q, Zhu W (2019) Application of neurite orientation dispersion and density imaging to characterize brain microstructural abnormalities in type-2 diabetics with mild cognitive impairment. J Magn Reson Imaging 50(3):889–898. https://doi.org/10.1002/jmri.26687
31. Atwal JK, Pinkston-Gosse J, Syken J, Stawicki S, Wu Y, Shatz C, Tessier-Lavigne M (2008) PirB is a functional receptor for myelin inhibitors of axonal regeneration. Science 322(5903):967–970. https://doi.org/10.1126/science.1161151
32. Liu Y, Ma C, Li H, Shen H, Li X, Fu X, Wu J, Chen G (2019) Nogo-A/Pir-B/TrkB signaling pathway activation inhibits neuronal survival and axonal regeneration after experimental intracerebral hemorrhage in rats. J Mol Neurosci 69(3):360–370. https://doi.org/10.1007/s12031-019-01365-1
33. Wang F, Cui H, Su Y, Zhao SG, Teng Y (2010) Expression change of PirB in mice retina after optic nerve injury. Mol Med Rep 3(3):405–407. https://doi.org/10.3892/mmr_00000272
34. Leterrier C (2018) The axon initial segment: an updated viewpoint. J Neurosci 38(9):2135–2145. https://doi.org/10.1523/JNEUROSCI.1922-17.2018
35. Harty RC, Kim TH, Thomas EA, Cardamone L, Jones NC, Petrou S, Wimmer VC (2013) Axon initial segment structural plasticity in animal models of genetic and acquired epilepsy. Epilepsy Res 105(3):272–279. https://doi.org/10.1016/j.eplepsyres.2013.03.004
36. Nelson AD, Caballero-Floran RN, Rodriguez Diaz JC, Hull JM, Yuan Y, Li J, Chen K, Walder KK, Lopez-Santiago LF, Bennett V, McInnis MG, Isom LL, Wang C, Zhang M, Jones KS, Jenkins PM (2020) Ankyrin-G regulates forebrain connectivity and network synchronization via interaction with GABARAP. Mol Psychiatry 25(11):2800–2817. https://doi.org/10.1038/s41380-018-0308-x
37. Marin MA, Ziburkus J, Jankowsky J, Rasband MN (2016) Amyloid-beta plaques disrupt axon initial segments. Exp Neurol 281:93–98. https://doi.org/10.1016/j.expneurol.2016.04.018
38. Rasband MN (2010) The axon initial segment and the maintenance of neuronal polarity. Nat Rev Neurosci 11(8):552–562. https://doi.org/10.1038/nrn2852
39. Clark K, Sword BA, Dupree JL (2017) Oxidative stress induces disruption of the axon initial segment. ASN Neuro 9(6):1759091417745426. https://doi.org/10.1177/1759091417745426
40. Huang CY, Rasband MN (2018) Axon initial segments: structure, function, and disease. Ann N Y Acad Sci 1420(1):46–61. https://doi.org/10.1111/nyas.13718
41. Grubb MS, Burrone J (2010) Activity-dependent relocation of the axon initial segment fine-tunes neuronal excitability. Nature 465(7301):1070–1074. https://doi.org/10.1038/nature09160
42. Dickson HM, Zurawski J, Zhang H, Turner DL, Vojtek AB (2010) POSH is an intracellular signal transducer for the axon outgrowth inhibitor Nogo66. J Neurosci 30(40):13319–13325. https://doi.org/10.1523/JNEUROSCI.1324-10.2010
43. Fujita Y, Endo S, Takai T, Yamashita T (2011) Myelin suppresses axon regeneration by PIR-B/SHP-mediated inhibition of Trk activity. EMBO J 30(7):1389–1401. https://doi.org/10.1038/emboj.2011.55
44. Zhao Z-h, Deng B, Xu H, Zhang J-f, Mi Y-j, Meng X-z, Gou X-c, Xu L-x (2016) PirB overexpression exacerbates neuronal apoptosis by inhibiting TrkB and mTOR phosphorylation after oxygen and glucose deprivation injury. Cell Mol Neurobiol 37(4):707–715. https://doi.org/10.1007/s10571-016-0406-8
45. Bi YY, Quan Y (2018) PirB inhibits axonal outgrowth via the PI3K/Akt/mTOR signaling pathway. Mol Med Rep 17(1):1093–1098. https://doi.org/10.3892/mmr.2017.7930
46. Lu XM, Mao M, Xiao L, Yu Y, He M, Zhao GY, Tang JJ, Feng S, Li S, He CM, Wang YT (2019) nucleic acid vaccine targeting Nogo-66 receptor and paired immunoglobulin-like receptor B as an immunotherapy strategy for spinal cord injury in rats. Neurotherapeutics 16(2):381–393. https://doi.org/10.1007/s13311-019-00718-3
47. Zhang Z, Wang Z, Ling Z, Li Y, Pan J, Gao Q, Zhang J, Yan L, Zhang Z, Li J (2021) A screened PirB antagonist peptide antagonizes Aβ42-mediated inhibition of neurite outgrowth in vitro. Applied Microbiology and Biotechnology:105 (11):4649–4662. https://doi.org/10.1007/s00253-021-11363-2
48. Ganguly K, Poo MM (2013) Activity-dependent neural plasticity from bench to bedside. Neuron 80(3):729–741. https://doi.org/10.1016/j.neuron.2013.10.028